Combined immunodeficiency caused by a loss-of-function mutation in DNA polymerase delta 1

Ye Cui, PhD,[a] Sevgi Keles, MD,[b] Louis-Marie Charbonnier, PhD,[a] Amélie M. Julé, PhD,[a] Lauren Henderson, MD, MSc,[a] Seyma Celikbilek Celik, BSc,[b] Ismail Reisli, MD,[b] Chen Shen, PhD,[c,d] Wen Jun Xie, PhD,[e] Klaus Schmitz-Abe, PhD,[f] Hao Wu, PhD,[a,c] and Talal A. Chatila, MD, MSc[a] *Boston and Cambridge, Mass, and Konya, Turkey*

GRAPHICAL ABSTRACT

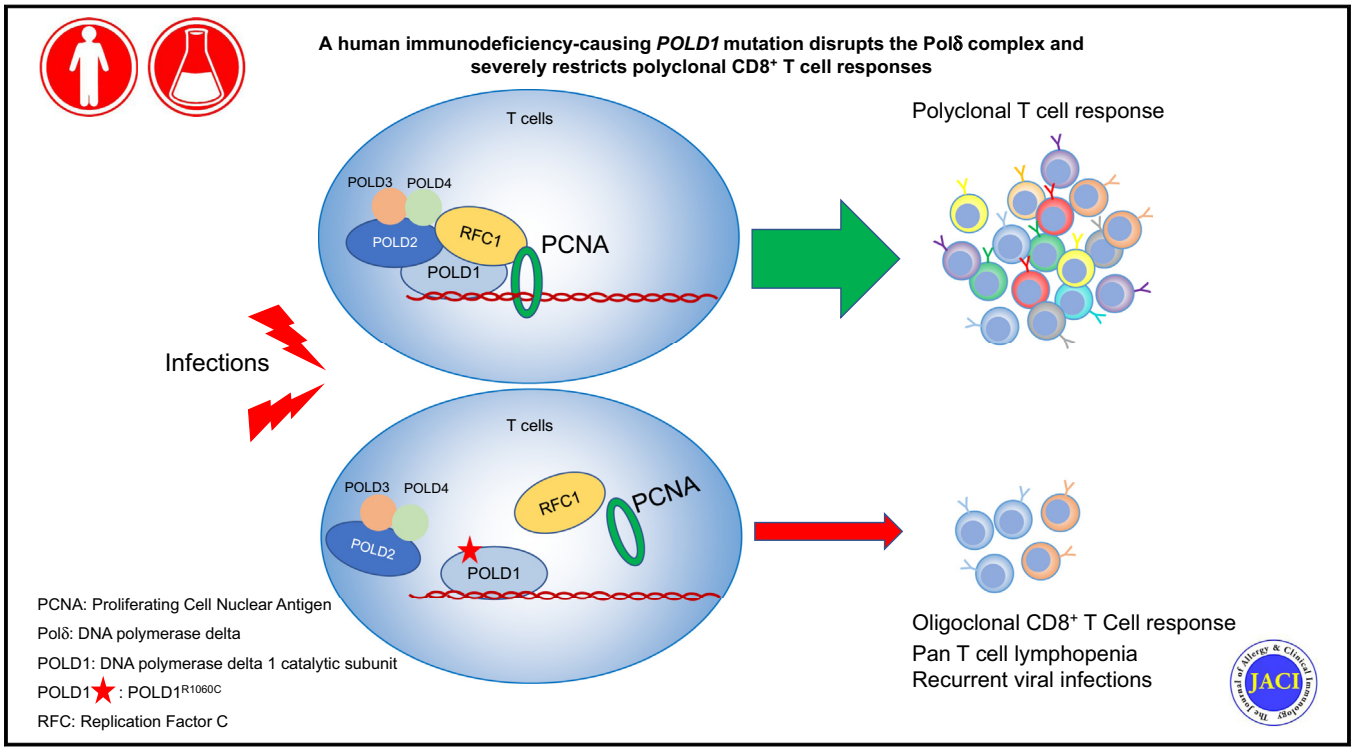

Background: Mutations affecting DNA polymerases have been implicated in genomic instability and cancer development, but the mechanisms by which they can affect the immune system remain largely unexplored.

Objective: We sought to establish the role of DNA polymerase δ1 catalytic subunit *(POLD1)* as the cause of a primary immunodeficiency in an extended kindred.

Methods: We performed whole-exome and targeted gene sequencing, lymphocyte characterization, molecular and functional analyses of the DNA polymerase δ (Polδ) complex, and T- and B-cell antigen receptor repertoire analysis.

Results: We identified a missense mutation (c. 3178C>T; p.R1060C) in *POLD1* in 3 related subjects who presented with recurrent, especially herpetic, infections and T-cell lymphopenia with impaired T-cell but not B-cell proliferation. The mutation destabilizes the Polδ complex, leading to ineffective recruitment of replication factor C to initiate DNA replication. Molecular dynamics simulation revealed that the R1060C mutation

From [a]the Division of Immunology, Boston Children's Hospital, and the Department of Pediatrics, Harvard Medical School, Boston; [b]Necmettin Erbakan University, Meram Medical Faculty, Division of Pediatric Allergy and Immunology, Konya; [c]the Program in Molecular and Cellular Medicine, Department of Pediatrics, and [f]the Division of Newborn Medicine and Neonatal Genomics Program, Boston Children's Hospital, Harvard Medical School, Boston; [d]the Department of Biological Chemistry and Molecular Pharmacology, Harvard Medical School; and [e]the Department of Chemistry, Massachusetts Institute of Technology, Cambridge.

This work was supported by National Institutes of Health grants 5R01AI085090 and 5R01AI128976 (to T.A.C.).

Disclosure of potential conflict of interest: The authors declare that they have no relevant conflicts of interest.

Received for publication July 5, 2019; revised September 11, 2019; accepted for publication October 4, 2019.

Available online October 16, 2019.

Corresponding author: Talal A. Chatila, MD, MSc, Division of Immunology, Boston Children's Hospital, and the Department of Pediatrics, Harvard Medical School, Karp Family Building, Rm 10-214, 1 Blackfan St, Boston, MA 02115. E-mail: talal.chatila@childrens.harvard.edu.

The CrossMark symbol notifies online readers when updates have been made to the article such as errata or minor corrections

0091-6749/$36.00

https://doi.org/10.1016/j.jaci.2019.10.004

disrupts the intramolecular interaction between the POLD1 CysB motif and the catalytic domain and also between POLD1 and the Polδ subunit POLD2. The patients exhibited decreased numbers of naive CD4 and especially CD8 T cells in favor of effector memory subpopulations. This skewing was associated with oligoclonality and restricted T-cell receptor β-chain V-J pairing in $CD8^+$ but not $CD4^+$ T cells, suggesting that $POLD1^{R1060C}$ differentially affects peripheral $CD8^+$ T-cell expansion and possibly thymic selection.
Conclusion: These results identify gene defects in *POLD1* as a novel cause of T-cell immunodeficiency. (J Allergy Clin Immunol 2020;145:391-401.)

Key words: *DNA polymerase delta 1, DNA polymerase δ1 catalytic subunit, replication factor C, POLD1, primary immunodeficiency-whole-exome sequencing*

DNA replication is a fundamental process for maintaining cellular homeostasis.[1] DNA polymerase delta (Polδ), one of the 3 family B polymerases in eukaryotes, is essential for leading and lagging strand synthesis.[2-4] In mammals polymerase δ is a heterotetramer that includes 4 subunits: POLD1 to POLD4.[5] DNA polymerase δ1 catalytic subunit (POLD1) functions as the catalytic subunit, which is endowed with both polymerase and exonuclease activities and plays a critical role in several synthetic and DNA-repair processes.[6,7] Total POLD1 deficiency is embryonically lethal in mice, whereas deficiency of POLD1 exonuclease activity in *Pold1*$^{exo/exo}$ mice (mutator mice) results in a high rate of DNA replication errors.[8] POLD2, POLD3, and POLD4 are accessory subunits that interact with other nuclear proteins to regulate the activity and stability of the Polδ complex.[9-11] In particular, POLD2 serves as a scaffold by interacting with POLD1 and the other Polδ subunits.[12] Additionally, the Polδ complex coordinately interacts with a number of proteins that enable its function, including DNA replication factor C (RFC) and proliferating cell nuclear antigen (PCNA).[13]

Studies have shown that mutations in *POLD1* in mice and human subjects lead to genomic instability, a hypermutator phenotype, and carcinogenesis.[14-16] Damaging heterozygous mutations in the POLD1 proofreading (exonuclease) domain have been identified in patients with inherited colorectal cancers.[17] A *POLD1* heterozygous single-amino-acid deletion that maps to the catalytic domain and that abrogates the DNA polymerase but not exonuclease activity has been identified in patients with a developmental disorder of mandibular hypoplasia, sensorineural hearing loss, progeroid features, and lipodystrophy with insulin resistance.[18,19] Thus mutations affecting different domains of POLD1 give rise to distinct disorders and phenotypes.

Here we identify a novel *POLD1* mutation that affects the stability of the Polδ complex, resulting in a disorder distinct from those caused by other POLD1 mutations. The patients presented with a combined immunodeficiency disorder associated with T-cell lymphopenia, $CD8^+$ T-cell oligoclonality, and repertoire restriction, which is indicative of a particularly important role for POLD1 in CD8 T-cell expansion.

Abbreviations used

BrdU:	Bromodeoxyuridine/5-bromo-2′-deoxyuridine
CDR3:	Complementarity-determining region 3
IGH:	Immunoglobulin heavy chain
LRTI:	Lower respiratory tract infection
MD:	Molecular dynamics
PCNA:	Proliferating cell nuclear antigen
Polδ:	DNA polymerase δ
POLA1:	DNA polymerase α1 catalytic subunit
POLBc:	DNA polymerase type B family catalytic domain
POLD1:	DNA polymerase δ1 catalytic subunit
POLE2:	DNA polymerase ε subunit 2
RFC:	Replication factor C
SHM:	Somatic hypermutation
TCR:	T-cell receptor
T_{EMRA}:	$CD45RA^+$ effector memory T
TRB:	T-cell receptor β chain
Treg:	Regulatory T
URTI:	Upper respiratory tract infection
VDJ:	Variable, diversity, and joining
VExP:	Variant Explorer Pipeline
WES:	Whole-exome sequencing
WT:	Wild-type

METHODS

Patient studies

All study participants were recruited after obtaining informed consent at the referring institution (Necmettin Erbakan University, Meram Medical Faculty, Konya, Turkey), and the studies were conducted at the Boston Children's Hospital under approved protocol #04-09-113R.

Whole-exome sequencing

Whole-exome sequencing (WES) was performed on genomic DNA of 2 affected siblings (P1 and P2), their parents, and their healthy sister through Axeq (Rockville, Md). The Agilent SureSelect Target enrichment kit was used for exon capture (Agilent Technologies, Santa Clara, Calif). Paired-end sequencing was performed with an Illumina HiSeq2000 instrument (Illumina, San Diego, Calif), which generated 150-bp reads. Average coverage in WES was 53 times, covering 96% of the coding regions.

Analysis of WES data was performed with the Variant Explorer Pipeline (VExP)[20] to narrow down potential candidate variants. VExP is a validated comprehensive system that integrates existing methods, genetic information, and probabilistic models into an automated pipeline for identification of disease genes. Raw data were processed, filtered, and analyzed according to VExP recommendations (see the Methods section in this article's Online Repository at www.jacionline.org).

Candidate genes that passed the criteria for the 2 affected samples were further evaluated by our research team (see Table E1 in this article's Online Repository at www.jacionline.org). The identified *POLD1* c. 3178C>T mutation was confirmed by means of Sanger sequencing by first generating a 404-bp amplicon from genomic DNA using the following primers: forward primer, 5′-AGAAGCTGGGATTGGCAGT-3′; reverse primer, 5′-GAGAGGCCTTGGAGTCAGAG-3′. The amplicon was then sequenced for the presence of the mutation using the following primer: 5′-GCCTACAT GAAGTCGGAGGA-3′. Sanger sequencing analysis was also used to screen other family members for the *POLD1* mutation.

Antibodies and flow cytometry

Anti-human mAbs to the following antigens were used for staining: CD3 (SK7), CD4 (SK3), CD8 (SK1), CD45RA (HI100), CD45RO (UCHL1), CCR7 (150503), CD31 (L133.1), T-cell receptor (TCR) α/β (WT31) and TCR γ/δ (11F2), CD16+CD56 (B73, 1MY3I), CD19 (SI25C1), IgD (IA6-2), and CD27 (L128; BD Biosciences, San Jose, Calif) and appropriate isotype controls. The mAb against POLD1 (sc-17776) was obtained from Santa Cruz Biotechnology, Santa Cruz, California. Antibodies against V5 were purchased from BioLegend (San Diego, Calif; 903801), POLD2 (HPA026745) and RFC1 (HPA046116) were purchased from Sigma-Aldrich (St Louis, Mo), POLD3 (A301-244A-M) was from Bethyl Laboratories (Montgomery, Tex), and β-actin was from Cell Signaling Technology (Danvers, Mass). Whole blood was

incubated with mAbs against surface markers for 30 minutes on ice. Intracellular staining with forkhead box P3 was performed by using eBioscience Fixation/Permeabilization buffer (eBioscience, San Diego, Calif), according to the manufacturer's instructions. Data were collected with a Fortessa cytometer (BD Biosciences) and analyzed with FlowJo software (TreeStar, Ashland, Ore).

Cell culture and transfection

HEK293T cells (ATCC, Manassas, Va) and fibroblasts were cultured with Dulbecco modified Eagle medium (Invitrogen, Carlsbad, Calif) plus 10% FBS (Gibco, Carslbad, Calif) supplemented with 1% penicillin-streptomycin (Invitrogen). Peripheral blood samples (5 mL) were collected from each subject and stored in tubes containing EDTA. PBMCs were isolated by using Ficoll-Paque PLUS (GE Healthcare, Chicago, Ill) gradient centrifugation and cultured in RPMI 1640 with 10% FBS and 1% penicillin-streptomycin (with nonessential amino acid, sodium pyruvate) with anti-CD3/CD28 beads (Invitrogen). B-cell proliferation was quantified by culturing PBMCs after stimulation with anti-CD40 mAb (10 μg/mL; 6245-CL-050; R&D Systems, Minneapolis, Minn) plus IL-21 (30 ng/mL; 200-21; PeproTech, Rocky Hill, NJ) for 5 days. Lipofectamine 2000 (Invitrogen) was used for transient transfection of HEK293T cells, according to the manufacturer's instructions.

Bromodeoxyuridine/5-bromo-2′-deoxyuridine cell proliferation assay

The bromodeoxyuridine/5-bromo-2′-deoxyuridine (BrdU) incorporation assay in the patients' PBMCs was performed with the Phase-Flow FITC BrdU Kit from BioLegend (catalog no. 370704), according to the manufacturer's instructions. The same kit included 7-aminoactinomycin D for total DNA staining.

Lentiviral transfections

HEK293T cells plated on 100-mm dishes were transfected with the indicated lentiviral expression plasmid (14 μg) together with GAG (10 μg), REV (5 μg), and VSV (2 μg). After 48 hours, viral particles were collected, filtered with a 0.45-μm membrane filter, and used to infect the indicated cells in the presence of polybrene (6 μg/mL). After transfection for 48 hours, cells were cultured in complete RPMI 1640 and were ready for the BrdU assay.

Plasmids

*POLD1*_pLX307 and pLX307 vectors were purchased from Addgene (Cambridge, Mass). The *POLD1* C3178T mutation was introduced into the *POLD1* plasmid with the Q5 Site-Directed Mutagenesis Kit (NEB, Ipswich, Mass) by using the following primers: forward, 5′-GCAGTGCCAGtGCTGC CAGGG-3′; reverse, 5′-GTCCAGAGGCGCGAGAAGC-3′. *POLD1* mutants were confirmed by using Sanger sequencing.

Immunoprecipitation assay and immunoblot analysis

For the immunoprecipitation assay, cell extracts were prepared with RIPA buffer (50 mmol/L Tris-HCl [pH 7.4], 150 mmol/L NaCl, 1 mmol/L EDTA, 1% Triton X-100, 0.1% SDS, and 0.5% deoxycholate) supplemented with a complete protease inhibitor cocktail (Roche, Mannheim, Germany) and a PhosSTOP phosphatase inhibitor cocktail (Roche). Lysates were incubated with the appropriate antibody for 4 hours up to overnight at 4°C before adding protein A/G agarose for 2 hours. Immunoprecipitates were washed 3 times with the same buffer and eluted with SDS loading buffer by boiling for 5 minutes.

For immunoblot analysis, samples were subjected to SDS-PAGE. Resolved proteins were then electrically transferred to a polyvinylidene difluoride membrane (Millipore, Temecula, Calif). Immunoblotting was probed with the indicated antibodies. Protein bands were visualized by using a SuperSignal West Pico chemiluminescence ECL kit (Pierce). Signal intensities of immunoblot bands were quantified by using ImageJ software (National Institutes of Health, Bethesda, Md).

Molecular modeling and simulation

We performed molecular dynamics (MD) simulation for the wild-type (WT) and mutant POLD1 to relax the protein structure obtained from homolog modeling. The simulation region starts from the 795th residue. All MD simulations were performed with the AMBER 14 suite.[21] POLD1 protein was immersed in a simulated water box, with the initial structure taken from molecular docking. The force field for protein is the AMBER parm10 force field,[21] and the SPC/E model was adopted for water.[22] Chloride ions were added to neutralize the system with a force field obtained from Joung and Cheatham.[23] The sizes of the simulation boxes are about 81 Å × 65 Å × 93 Å. For the WT and mutant POLD1, we carried out NPT ensemble simulation with a 10-ns-long trajectory after initial equilibration. The Berendsen weak-coupling barostat was used to control the pressure at 1 bar.[24] The temperature was controlled by using Langevin dynamics at 300 K. The SHAKE algorithm was used to constrain all bonds involving hydrogen atoms.[25] A cutoff of 10.0 was adopted for nonbonding interactions. For long-range electrostatic interactions, the Particle-Mesh Ewald method was applied.

Overall protein secondary and tertiary structures persist during the simulation, suggesting that homolog modeling provides a good prediction of POLD1's structure. A hydrogen bond is considered formed only if the distance between the heavy atom of the hydrogen bond donor and acceptor is less than 3.5 Å and the N–H–O angle is greater than 135°.

Repertoire analysis

$CD4^+$ T ($CD3^+CD4^+$) cells, $CD8^+$ T ($CD3^+CD8^+$) cells, and B ($CD3^-CD19^+$) cells were isolated from fresh PBMCs obtained from $POLD1^{R1060C}$ patients and healthy control subjects. Genomic DNA was isolated with the QIAamp DNA Blood Mini Kit (Qiagen, Hilden, Germany) and sent to Adaptive Biotechnologies (Seattle, Wash) for immune repertoire analysis. A multiplex PCR protocol was used to amplify the complementarity-determining region 3 (CDR3) of the sorted lymphocytes by using a standard quantity of DNA as the template. The Illumina platform (Illumina, San Diego, Calif) was used for sequencing of the PCR products. Sequences were aligned to a reference genome, and T-cell receptor β chain *(TRB)* and immunoglobulin heavy chain (*IGH*) variable, diversity, and joining (VDJ) gene definitions were based on the International ImMunoGeneTics system.[26] Data were filtered and clustered by using the relative frequency ratio between similar clones and a modified nearest-neighbor algorithm to merge closely related sequences and remove both PCR and sequencing errors, as previously described.[27,28] Productive unique and total sequences were analyzed for TCR and BCR V, D, and J usage with the ImmunoSEQ Analyzer set of online tools and with R software (version 3.6.1). Physicochemical properties of amino acid sequences were analyzed by using the Alakazam package.[29] Sequencing of the *TRB* and *IGH* rearranged products was completed successfully in all samples (see Table E2 in this article's Online Repository at www.jacionline.org). Primary sequencing data are available at https://clients.adaptivebiotech.com/pub/cui-2019-jaci.

Statistical analysis

Aggregate results are presented as means ± SEMs. Comparison between groups was carried out with 1-way ANOVA with Bonferroni posttest analysis, as indicated. Differences in mean values were considered significant at a P value of less than .05.

RESULTS

Identification of a novel immunodeficiency associated with a novel POLD1 mutation

P1 is a 14-year-old girl born to consanguineous (first cousins) Turkish parents (Fig 1, *A*), who experienced recurrent upper respiratory tract infections (URTIs) and lower respiratory tract infections (LRTIs) starting early in life. At 3 years of age, she

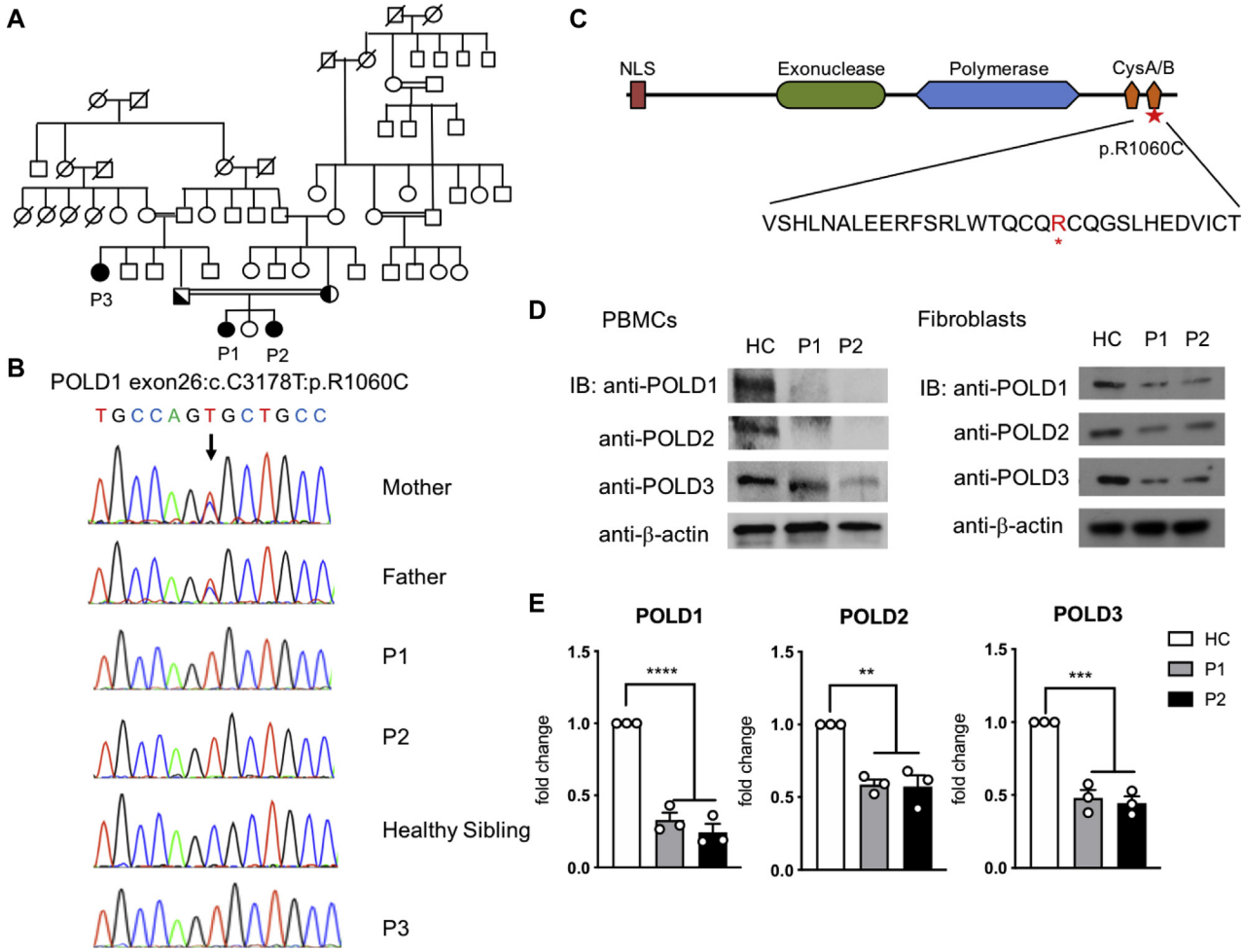

FIG 1. Characterization of a POLD1 mutation in kindred with combined immunodeficiency. **A,** Patient pedigree and familial segregation of the mutant *POLD1* allele. *Double lines* connecting parents indicate consanguinity. Probands are indicated as P1 to P3. *Squares*, Male subjects; *circles*, female subjects; *solid symbols*, patients; *half-filled symbols*, heterozygous. **B,** Sanger sequencing fluorograms of the germline c.3178C>T *POLD1* mutation in patients P1 to P3 and the parents of P1 and P2 compared with the equivalent DNA sequences in an unaffected healthy sibling. **C,** Schematic representation of POLD1 protein. Different domains are depicted as follows: the nuclear localization signal *(NLS)* in red, the exonuclease in light green, the polymerase domain in light blue, and the cysteine-rich metal-binding domains *(CysA/B)* in orange. The identified R1060C mutation and its position within the CysB polypeptide sequence are indicated by a *red star*. **D,** Immunoblot *(IB)* analysis of POLD1/2/3 protein expression in PBMCs *(left)* and primary fibroblasts *(right)* of P1, P2, and a healthy control subject *(HC)*. **E,** Quantitation of POLD1/2/3 protein expression in primary fibroblasts of P1 and P2 normalized for β-actin expression and expressed as fold change compared with that of HC fibroblasts (n = 3; *open circles*). Results represent means ± SEMs. $^{**}P < .01$, $^{***}P < .001$, and $^{****}P < .0001$, 1-way ANOVA with Bonferroni posttest analysis.

received a diagnosis of sensorineural hearing loss after evaluation for language delay. She underwent adenotonsillectomy at 5½ years of age because of recurrent URTIs and serous otitis media. She had severe chickenpox at 6 years of age that eventually resolved. Thereafter, she started experiencing LRTIs at a frequency of 4 to 5 times per year, mainly in winter, requiring intravenous antibiotic therapy.

Starting at age 9 years, she had recurrent oral herpes infections every 1 to 2 months, as well as several episodes of recurrent herpes zoster for which she received acyclovir therapy. Investigation into her recurrent herpetic infections revealed marked lymphopenia, for which she was referred for immunologic evaluation at 12 years of age.

Her immunologic workup was particularly notable for profound $CD3^+CD4^+$ lymphopenia. She had mildly decreased serum IgG and low IgA and IgM antibody concentrations, whereas her tetanus vaccine–related antibody responses were absent despite having been fully vaccinated (Table I). She was started on immunoglobulin replacement therapy, which resulted in resolution of LRTIs and markedly decreased herpetic infections.

Patient P2 is the younger sister of P1 and presented at age 3 years with a history of fever and cough. Her weight (12.3 kg [10th-25th percentile]) and height (98 cm [50th-75th percentile]) were in normal range for her age. Her laboratory results revealed marked lymphopenia, hypogammaglobulinemia, and low

TABLE I. Hematologic and immunologic parameters in patients with the *POLD1*^{R1060C} mutation

	Patient 1			Patient 2				Patient 3	
Age	12 y	13 y (on IVIG)	Normal range for age	3 y	4 y	5 y	Normal range for age	29 y	Normal range for age
CBC									
WBC (cells/μL)	4,300	4,860	4,500-13,000	3,260	3,070	1,830	5,000-14,500	6,720	4,000-10,000
Neutrophils (cells/μL)	3,100	3,430	1,500-7,300	1,970	1,740	900	1,500-8,000	5,370	1,500-7,300
Lymphocytes (cells/μL)	600	430	1,200-5,200	765	971	470	1,500-7,000	780	800-5,500
Eosinophils (cells/μL)	20	260	200-600	2	134	130	200-600	70	200-600
Hemoglobin (g/dL)	12.8	14.2	12.1-17.2	13.0	13.1	13	11.1-17.2	11.9	12.1-17.2
Platelets (cells/μL)	344,000	348,000	150,000-400,000	360,000	323,000	244,000	150,000-400,000	152,000	150,000-400,000
Immunoglobulins									
IgA (mg/dL)	23	23	72-177	26	28		46-129	42.1	65-176
IgM (mg/dL)	49	55	63-164	97	97		50-146	126	86-175
IgG (mg/dL)	723	911	822-1,323	588	568		722-1,195	902	944-1,506
IgE (IU)	17	19		18	19		68	18	
Specific antibody response									
Anti-tetanus IgG (IU/mL)	0.01	0.65	>0.1	0.01	0.2*		>0.1	0.1	>0.1
Isohemagglutinin titer (dilutions)	1/16	1/16	>1/16	1/32	1/64		>1/16	1/16	>1/16
Anti–hepatitis B antibodies (IU)	319		>10	38	624		>10	0.06	>10
Lymphocyte subset analysis									
$CD3^+$ (cells/μL)	330	177	1,000-2,600	337	437	100	1,400-6,200	252	1,000-2,600
$CD3^+CD4^+$ (cells/μL)	102	66	530-1,500	145	184	57	700-2,200	101	530-1,500
$CD3^+CD8^+$ (cells/μL)	186	89	330-1,100	176	233	105	490-1,300	135	330-1,100
$CD19^+$ (cells/μL)	120	151	110-570	337	456	239	390-1,400	85	110-570
$CD16^+CD56^+$ (cells/μL)	12	46	70-480	61	58	61	130-720	402	70-480
$CD3^+$TCR α/β^+ (cells/μL)	213		700-2,800		466		600-4,300		600-3,300
$CD3^+$ TCR γ/δ^+ (cells/μL)	54		39-540		39		27-960		25-200
$CD4^+CD45RA^+$ $CD31^+$ (%)	13.0		32.9-61.5		48.0		52-67	5	9.8-43.2
$CD19^+IgD^+CD27^-$ (%)		62.6	51.3-82.5			61.8	47.3-77.0	64	48.4-79.7
$CD19^+IgD^-CD27^+$ (%)	7.0	2.06	8.7-25.6		6.1	1.12	10.9-30.4	1.86	8.3-27.8
$CD19^+IgD^+CD27^+$ (%)		0.53	4.6-18.2			0.49	5.2-20.4	0.47	7.0-23.8
$CD19^+CD24^+$ $CD38^+$ (%)		5.48	5.3-18.9			4.43	7.4-23.7	0.7	2.2-13.3

IVIG, Intravenous immunoglobulin.
*Postbooster vaccination.

$CD3^+CD4^+$ T-cell numbers similar to her older sister (Table I). She also had an unprotective tetanus antibody response on initial presentation despite her prior vaccination that normalized on booster vaccination. She is currently 5 years of age and still has recurrent croup and oral herpes infections, for which she is treated symptomatically. Auditory testing revealed normal hearing.

P3 is a 29-year-old paternal aunt of P1 and P2 (Fig 1, *A*). She had encephalitis after a primary varicella infection at 3 years of age, from which she was left with mental retardation, hearing deficit, and speech delay. In the ensuing years she has had recurrent oral herpetic infections, for which she is treated symptomatically. She also has URTIs in the winter requiring oral antibiotic therapy.

Pedigree analysis suggested an autosomal recessive inheritance of the disease. To identify the underlying gene defect, we performed WES for the whole family. Knowing that the family is consanguineous, we executed homozygosity mapping by using their WES data (see the Methods section in this article's Online Repository). Five regions of homozygosity were identified, and only the largest found on chromosome 19 (14 Mb in size) contains mutations with a minor allele frequency of less than 0.01 that segregate within the family (see Fig E1 and Table E3 in this article's Online Repository at www.jacionline.org). Of the 9 genes identified in this region, including 6 candidate genes with homozygous recessive mutations, the most promising was a homozygous C>T substitution in exon 26 of *POLD1* (c.3178C>T; p.R1060C; based on POLD1 isoform 1, NM_001256849.1; see Table E1). This missense homozygous mutation has not been previously reported in the genomAD, ExAC, dbSNP, or 1000 Genomes Project databases and was confirmed by using Sanger sequencing (Fig 1, *B*). Both parents were heterozygous for the mutation. Her sister (P2), who also

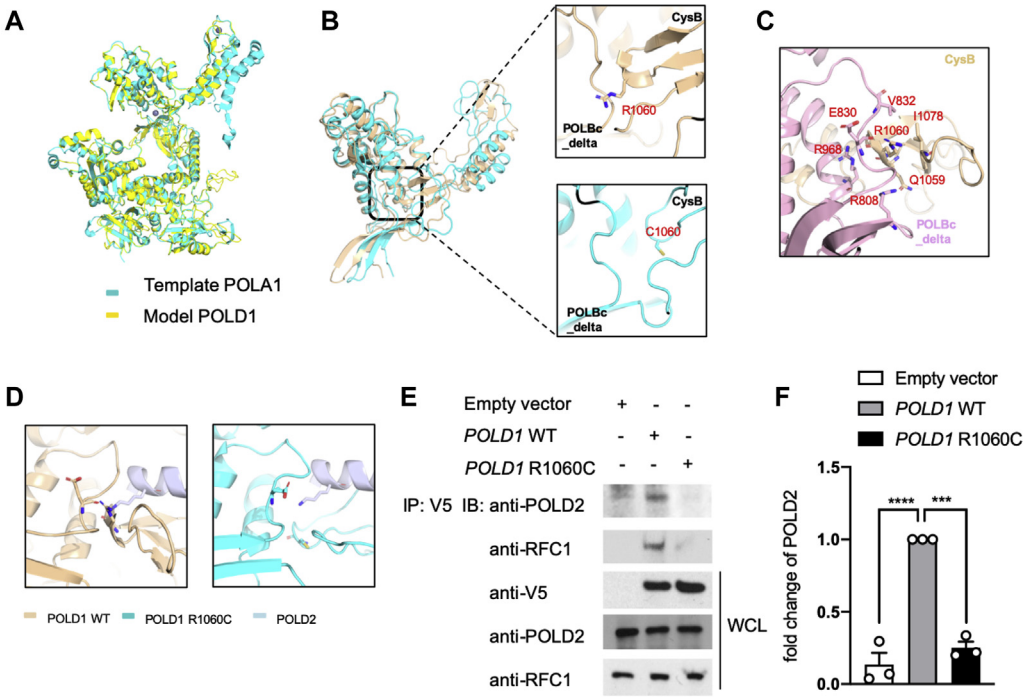

FIG 2. The POLD1^{R1060C} mutation disrupts POLD1-intrinsic and POLD1-POLD2 molecular interactions. **A,** Protein structure model of full-length POLD1 using Swiss modeling based on the crystal structure of POLA1. **B,** Distance between the CysB motif and the POLBc_delta domain in WT POLD1 and the POLD1^{R1060C} mutant protein are measured by using 10-ns snapshots. **C,** Detailed interface analysis of POLD1's structure. Hydrogen bonds between E830 and R1060, R968 and R1060 backbone, and R808 and Q1059 are shown in blue and red. **D,** Docking model showing cooperation between the CysB motif and the POLBc_delta domain in recruiting POLD2 and its disruption by the R1060C mutation. **E,** HEK293T cells were transfected with the indicated plasmids. Twenty-four hours after transfection, cell lysates were immunoprecipitated with an anti-V5 antibody and then immunoblotted *(IB)* with the indicated antibodies. *WCL*, Whole cell lysate. **F,** Quantitation of co-immunoprecipitated POLD2 protein by empty vector, WT POLD1, and POLD1^{R1060C} in Fig 2, *E*, expressed as fold change compared with that of WT POLD1 (n = 3; *open circles*). Results represent means ± SEMs. ***P < .001 and ****P < .0001, 1-way ANOVA with Bonferroni posttest analysis.

had recurrent infections, was found to be homozygous for the same mutation by using Sanger sequencing, as was a paternal aunt (P3), who had early childhood encephalitis after varicella infection. A number of extended family members had colon and rectal cancers but did not carry the mutant allele.

The R1060C substitution localizes to the CysB motif at the C-terminus of POLD1, which was away from the exonuclease and polymerase domains (Fig 1, *C*). Immunoblot analysis revealed decreased POLD1 expression in P1 and P2 compared with that in their healthy sibling in PBMCs and fibroblasts (Fig 1, *D* and *E*). Levels of other components of the Polδ complex are also decreased, including POLD2 and POLD3. Thus the POLD1^{R1060C} mutation exerted a global effect on the Polδ complex.

POLD1^{R1060C} affects the stability of the polymerase δ complex

DNA polymerases have been classified into several families based on their amino acid sequences. In polymerase family B both Polα and Polδ are key enzymes for eukaryotic nuclear DNA replication.[30] The structure of the family B DNA polymerases has been conserved throughout evolution, although their primary sequence varies. The structure of the DNA polymerase α1 catalytic subunit (POLA1) is well studied.[31]

To clarify the role of the R1060C missense substitution in POLD1 from the family with immunodeficiency syndrome, we generated a model of full-length POLD1 using Swiss modeling based on the crystal structure of POLA1, which has a sequence identity of 25.9%. Most of the structural elements aligned well between the POLD1 model and the POLA1 structure, with an average root-mean-square deviation of 0.315 Å (Fig 2, *A*).

Based on the POLD1 model, we introduced the R1060C mutation in PyMol followed by MD simulation for the WT and mutant POLD1 to relax the protein structure obtained from homolog modeling with a time scale of 10 ns. The simulation region starts from residue 795 in consideration of domain of interests and computational cost. After we extracted 10-ns snapshots of WT POLD1 and the R1060C mutant protein, we found a significance distance change between the CysB motif and the DNA polymerase type B family catalytic subunit (POLBc) delta domain (Fig 2, *B*). The CysB motif in POLD1 shows an intact interaction with the POLBc delta domain while the C1060 mutant lost the interaction. Detailed interface analysis showed that hydrogen bonds between E830 and R1060, R968 and R1060 backbone, and R808 and Q1059 and the hydrophobic interaction between V832 and I1078 dominate the mutual interaction between these 2 domains (Fig 2, *C*). By calculating the distance between residue 1060 and 830 in WT and mutant POLD1, we found that the R1060-E830 interaction maintains a shorter

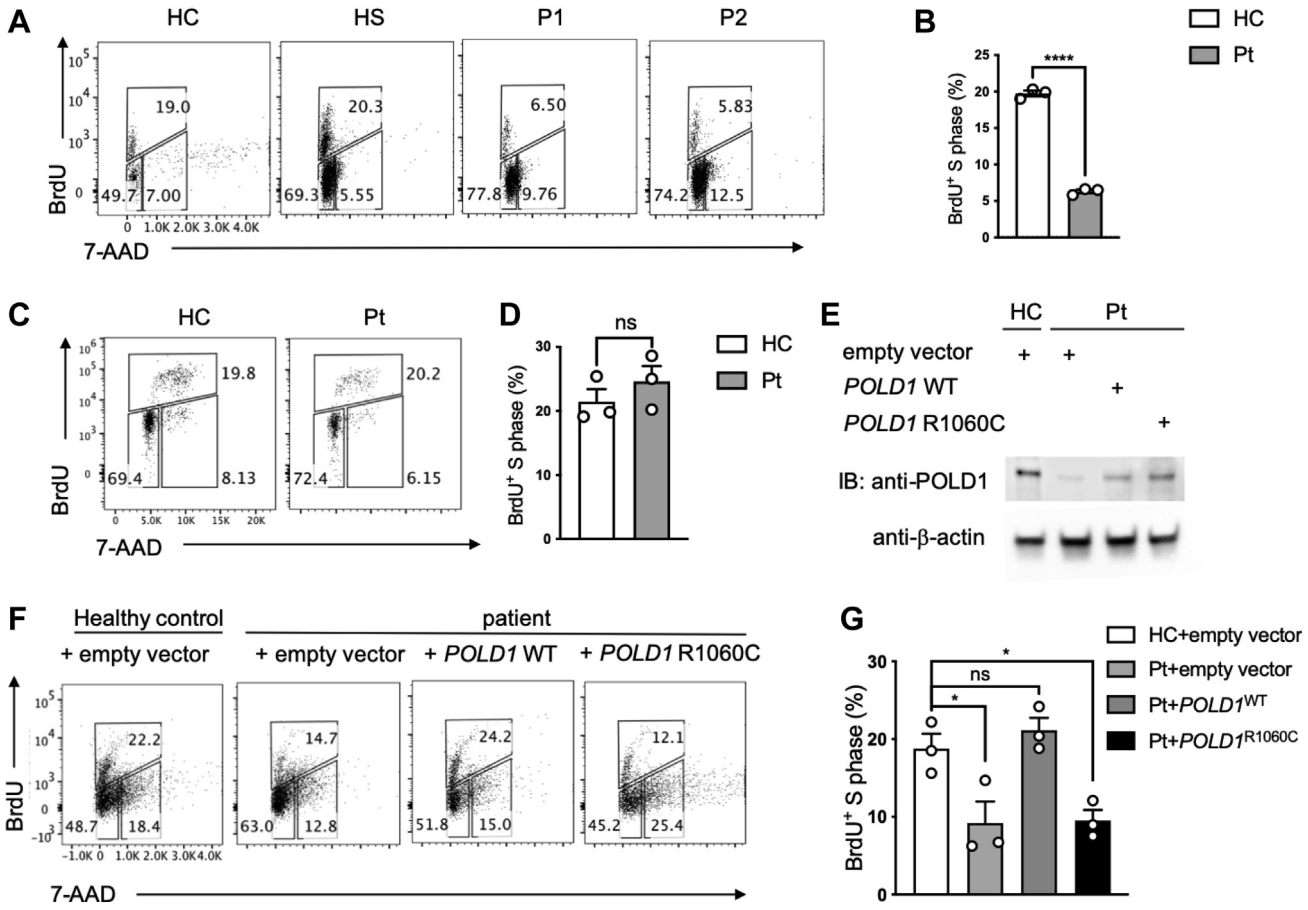

FIG 3. Defective proliferation of POLD1^{R1060C} T cells and its rescue by WT POLD1 expression. **A,** Representative flow cytometric analysis of BrdU^{+} P1 and P2 T cells versus those of a healthy control subject *(HC)* and the healthy sibling *(HS)*. **B,** Frequencies of BrdU^{+} T cells in healthy control subject versus P1 to P3 cell cultures (n = 3; *open circles*). **C,** Representative flow cytometric analysis of B cells from a BrdU^{+} patient *(Pt)* versus those of a healthy control subject *(HC)*. **D,** Frequencies of BrdU^{+} B cells in healthy control subject versus P1 to P3 cell cultures (n = 3; *open circles*). **E,** Immunoblot analysis of POLD1 expression in transduced cells. **F,** Representative dot plot analysis of T cells transfected with either empty vector, *POLD1* WT, or *POLD1* R1060C lentiviral plasmid. Data are representative of 3 experiments. **G,** Frequencies of BrdU^{+} T cells transfected with either empty vector, *POLD1* WT, or *POLD1* R1060C lentiviral plasmid in Fig 3, *F* (n = 3; *open circles*). Results are means ± SEMs. *7-AAD,* 7-Aminoactinomycin D. *ns,* Not significant. ****$P < .0001$, unpaired *t* test in Fig 3, *B* and *D*. *$P < .05$, 2-way ANOVA with Bonferroni posttest analysis in Fig 3, *G*.

distance than C1060-E830 after the structural relaxation (see Fig E2, *A*, in this article's Online Repository at www.jacionline.org), indicating that this interaction pair might be critical to maintain the CysB-POLBc_delta interaction. Also, hydrogen bond tracing revealed that the interaction between R1060 and E830 is highly stable during the whole simulation trajectory (see Fig E2, *B*), which provides further evidence that R1060 is critical for the intramolecular interaction of POLD1. Because of the decreased expression of POLD2 in patients' polymerase δ, we hypothesized that the POLD1^{R1060C} mutation affects the stability of the polymerase δ complex.

Considering that the weaker intramolecular interaction in the mutant protein might further affect the recruitment of downstream POLD subunits, we built both the WT and mutant model of the POLD1 10-ns snapshots/POLD2 complex based on the crystal structure of the POLA1/POLA2 complex (PDB ID: 5EXR). Overall, the docking model clearly indicated the cooperation between the CysB motif and the POLBc_delta domain in recruiting POLD2. This cooperative interaction is weakened by the R1060C mutant, which might disrupt POLD1:-POLD2 complex formation (Fig 2, *D*).

To validate the results obtained with molecular modeling, we examined the capacity of recombinant tagged WT and mutant POLD1 expressed in HEK293T cells to interact with the endogenous POLD2. Co-immunoprecipitation studies showed that the R1060C mutation interfered with formation of the POLD complex, as indicated by the capacity of WT POLD1 but not the POLD1^{R1060C} mutant protein to coprecipitate with POLD2 despite equal expression of the respective POLD1 proteins (Fig 2, *E* and *F*). Furthermore, we examined the capacity of POLD1^{R1060C} mutant protein to interact with other components of the DNA replication complex. During DNA replication, Polδ associates with RFC, a step necessary for loading PCNA onto DNA to initiate DNA replication. However, unlike WT POLD1, POLD1^{R1060C} did not effectively coprecipitate with RFC, which is indicative of poor association (Fig 2, *E*). Overall, these results

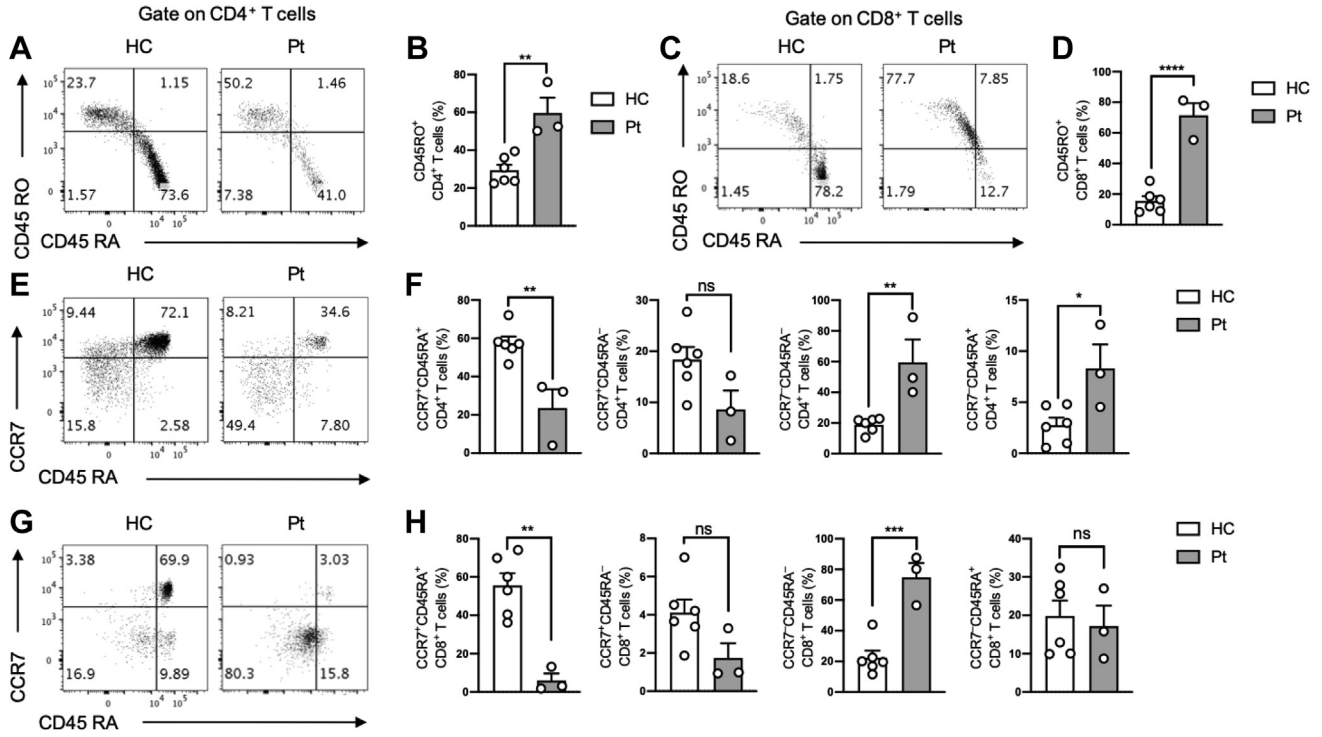

FIG 4. Increased frequency of memory T cells in patients with the POLD1^{R1060C} mutation. **A,** Flow cytometric analysis of circulating CD45RO$^-$CD45RA$^+$ and CD45RO$^+$CD45RA$^-$ CD4$^+$ T cells in a control subject and a patient with the POLD1^{R1060C} mutation. **B,** Frequency of activated CD45RO$^+$CD45RA$^-$ cells within the peripheral blood CD4$^+$ T-cell pool of control subjects and patients with the POLD1^{R1060C} mutation. **C,** Flow cytometric analysis of circulating CD45RO$^-$CD45RA$^+$ and CD45RO$^+$CD45RA$^-$ CD8$^+$ T cells in a control subject and a patient with the POLD1^{R1060C} mutation. **D,** Frequency of activated CD45RO$^+$CD45RA$^-$ cells within the peripheral blood CD8$^+$ T-cell pool of control subjects and patients with the POLD1^{R1060C} mutation. **E,** Flow cytometric analysis of circulating T_{EMRA} CD45RA$^+$CCR7$^-$ and naive CD45RA$^+$CCR7$^+$ CD4$^+$ T cells in a control subject and a patient with the POLD1^{R1060C} mutation. **F,** Frequency of circulating naive CD45RA$^+$CCR7$^+$, central memory CD45RA$^-$CCR7$^+$, effector memory CD45RA$^-$CCR7$^-$, and T_{EMRA} CD45RA$^+$CCR7$^-$ cells within the peripheral blood CD4$^+$ T-cell pool of control subjects and patients with the POLD1^{R1060C} mutation. **G,** Flow cytometric analysis of circulating T_{EMRA} CD45RA$^+$CCR7$^-$ and naive CD45RA$^+$CCR7$^+$ CD8$^+$ T cells in a control subject and a patient with the POLD1^{R1060C} mutation. **H,** Frequency of circulating naive CD45RA$^+$CCR7$^+$, central memory CD45RA$^-$CCR7$^+$, effector memory CD45RA$^-$CCR7$^-$, and T_{EMRA} CD45RA$^+$CCR7$^-$ cells within the peripheral blood CD8$^+$ T-cell pool of control subjects and patients with the POLD1^{R1060C} mutation. *HC*, Healthy control subject; *Pt*, patient. *ns*, Not significant. *$P < .05$ and ***$P < .001$, Student unpaired 2-tailed *t* test.

indicate that that the POLD1^{R1060C} mutation interfered with molecular interactions involved in Polδ assembly and formation of the overall DNA replication complex.

POLD1^{R1060C} results in lower cell proliferation

To determine whether the R1060C mutation in POLD1 affected DNA replication and cell proliferation, we analyzed the proliferative activities of T cells from control subjects and patients on treatment of PBMCs with anti-CD3 plus anti-CD28 mAb for 3 days, followed by a 4-hour stimulation with phorbol 12-myristate 13-acetate and ionomycin.[32] The cells were pulsed with BrdU, which labels newly synthesized DNA characteristic of the cell-cycle S phase.[33] Results showed that T cells, but not B cells, from patients were profoundly deficient in BrdU labeling after stimulation, which is indicative of poor S-phase DNA replication (Fig 3, *A-D*).

To determine whether the poor proliferation of patients' T cells was directly related to the POLD1 defect, we undertook rescue experiments in which patients' T cells were expanded with anti-CD3 plus anti-CD28 mAb treatment, followed by transfection with a lentiviral vector encoding either WT POLD1 or the POLD1^{R1060C} mutant. Both the WT POLD1 and the POLD1^{R1060C} mutant were equally expressed in the transfected cells (Fig 3, *E*). Results showed that DNA replication was rescued in WT POLD1–transduced patient cells, with a significant increase in the frequency of cells in the S phase, whereas the POLD1^{R1060C} mutation did not do so (Fig 3, *F* and *G*). Collectively, our studies indicate that the POLD1^{R1060C} mutant severely decreased DNA replication.

Increased frequency of memory T cells in patients with the POLD1^{R1060C} mutation

In view of their recurrent infections and immune disorder phenotypes, we further examined the cohort of patients with the POLD1^{R1060C} mutation for cell abnormalities. Consistently, all 3 patients with the POLD1^{R1060C} mutation showed sharp skewing

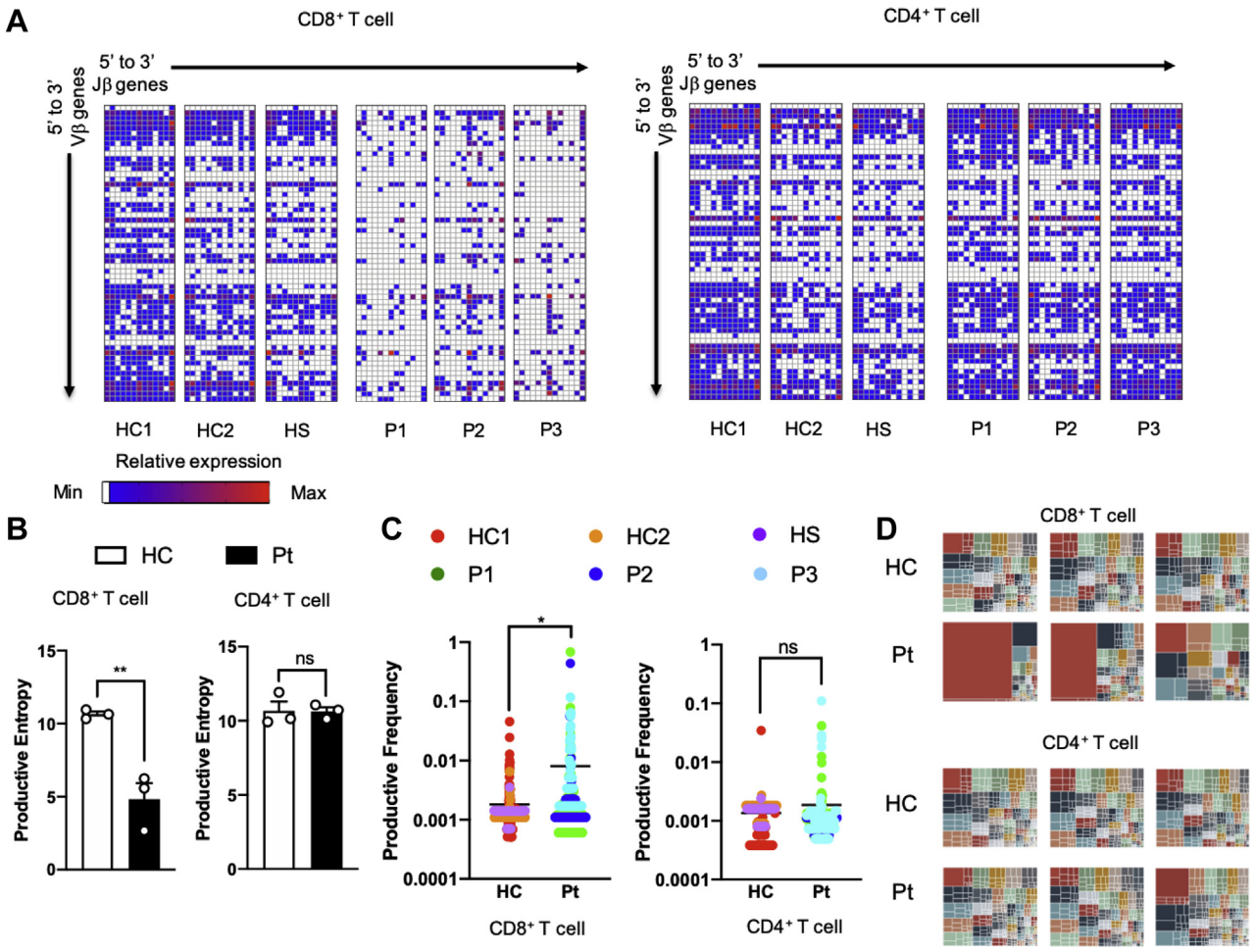

FIG 5. Restricted usage of Vβ and Jβ genes in T cells from patients with the POLD1^{R1060C} mutation. **A,** Frequencies of specific Vβ and Jβ pairing in unique *TRB* clonotypes of CD8$^+$ and CD4$^+$ T cells from healthy control subjects *(HC)* and patients *(Pt)*. *White areas* represent the absence of a given Vβ and Jβ pairing. *Blue areas* reflect a low frequency, and *red areas* represent a higher frequency of usage. **B,** Productive entropy of CD8$^+$ and CD4$^+$ T cells in healthy control subjects versus patients (n = 3; *open circles*). **C,** Productive frequencies of the top 100 most abundant clonotypes of CD8$^+$ and CD4$^+$ T cells in healthy control subjects versus patients. **D,** Tree map of clonality in CD8$^+$ and CD4$^+$ T cells. Each *square* represents a specific V-J pairing. The area of each square is proportional to the total frequency of the corresponding *TRB* clonotypes in each sample. *ns*, Not significant. **P* < .05 and ***P* < .01, Student unpaired 2-tailed *t* test.

of peripheral CD4 and CD8 T cells toward a memory (CD45RA$^-$CD45RO$^+$) phenotype (Fig 4, *A-D*). The frequencies of naive CD45RA$^+$CCR7$^+$ CD4$^+$ T cells and especially CD8$^+$ T cells were profoundly decreased in patients with the POLD1^{R1060C} mutation, whereas the frequencies of CD45RA$^-$CCR7$^-$CD4$^+$ and CD8$^+$ T cells (CD45RA$^-$ effector memory T cells) were increased. Frequencies of CD45RA$^+$CCR7$^-$ CD8$^+$ T cells (CD45RA$^+$ effector memory T [T_{EMRA}] cells) were similar in patients and control subjects, whereas frequencies of CD4$^+$ T_{EMRA} cells were marginally increased in patients. Frequencies of CD45RA$^-$CCR7$^+$ CD4$^+$ T cells (central memory T cells) and CD8$^+$ T cells were mildly decreased compared with those in the healthy control group without achieving statistical significance (Fig 4, *E-H*).

Flow cytometric analysis of regulatory T (Treg) cells in peripheral blood of patients with the POLD1^{R1060C} mutation showed a mild but nonsignificant increase in the distribution of CD4$^+$CD25^{hi}CD127^{lo} T cells (see Fig E3, *A* and *B*, in this article's Online Repository at www.jacionline.org). The percentage of induced Treg cells was found to be similar in patients with the POLD1^{R1060C} mutation and control subjects (see Fig E3, *C* and *D*). Expression of several canonical Treg cell markers, including Foxp3, cytotoxic T lymphocyte–associated antigen 4, and Helios, was normal in patients compared with control subjects (see Fig E3, *E*). Overall, these results establish a predominance of effector memory T-cell subpopulations in patients with the POLD1^{R1060C} mutation in the context of T-cell lymphopenia.

Restricted TCR V-J pairing in POLD1^{R1060C} CD8$^+$ T cells

Given that the POLD1^{R1060C} mutation gave rise to severe T lymphopenia with effector T-cell skewing, we examined the patients' CD4 and CD8 T-cell populations for evidence of abnormalities in their T-cell receptor repertoire. Specifically, we

asked whether POLD1 might play a role in the nonhomologous end-joining as, reflected in VDJ recombination. Accordingly, we analyzed *TRB* of cell-sorted $CD4^+$ and $CD8^+$ T cells and *IGH* of $CD19^+$ B cells for evidence of VDJ recombination defects and oligoclonality. Repertoire analysis showed that the V-J pairing patterns and productive entropy (a measure of clonal diversity) were similar between $CD4^+$ T and B cells from patients with the $POLD1^{R1060C}$ mutation and control subjects (Fig 5, *A* and *B*, and see Fig E4, *A* and *B*, in this article's Online Repository at www.jacionline.org). In contrast, the $POLD1^{R1060C}$ $CD8^+$ T-cell subset displayed restricted V-J gene combinations and lower productive entropy (Fig 5, *A* and *B*). Analysis of the productive frequencies of the top 100, as well as total clonotypes, further revealed severe oligoclonality among patients' $CD8^+$ but not $CD4^+$ T cells (Fig 5, *C* and *D*). Altogether, these observations suggested a selective effect of $POLD1^{R1060C}$ on CD8 T-cell clonal expansion in the periphery and possibly an additional effect during thymic development.

To determine whether POLD1 is involved in somatic hypermutation (SHM), we analyzed SHM patterns in B cells. We found no difference between patients and control subjects in the IGHV-IGHJ pairing, D gene use, productive entropy, and the proportion of unique *IGH* rearrangements carrying at least 1 mutation (see Fig E4, A-*D*). The rate of SHM in the V segment was similar in both of the productive *IGH* rearrangements and nonproductive *IGH* rearrangements of patients with the $POLD1^{R1060C}$ mutation (see Fig E4, *E*). Finally, the *in silico*–translated amino acid sequences of the *IGH* CDR3 region showed no differences in length and tyrosine content between patients with the $POLD1^{R1060C}$ mutation and healthy control subjects (see Fig E4, *F* and *G*), whereas the hydrophobicity analysis showed a borderline statistically significant marginal difference between patients with the $POLD1^{R1060C}$ mutation and healthy control subjects ($P = .049$; see Fig E4, *F*). These findings, together with the normal B-cell proliferation shown earlier, confirmed that the $POLD1^{R1060C}$ mutation spared the B-cell compartment.

DISCUSSION

In this study we report a homozygous missense mutation in *POLD1*, encoding the catalytic subunit of the ubiquitous Polδ, in 3 patients from an extended consanguineous kindred who presented with recurrent infections with T-cell lymphopenia and poor antibody responses. Functional and structural analysis indicated that the mutation impaired the interaction of POLD1 with other Polδ subunits, resulting in poor Polδ complex formation and defective DNA replication. Thus our results establish this mutation as a novel cause of primary combined immunodeficiency.

The mutant $POLD1^{R1060C}$ protein did not associate with the Polδ accessory subunit POLD2 or with the DNA replication complex component RFC, which is necessary for loading PCNA onto DNA to initiate DNA replication.[34] Structural modeling revealed the mutation disrupted a critical molecular interaction between POLD1 and POLD2, which is in agreement with the coprecipitation studies, showing failure of the mutant $POLD1^{R1060C}$ protein to associate with POLD2. Although the mutation is located at the C-terminus of POLD1 away from the catalytic and DNA exonuclease domains, a secondary effect of the mutation on the catalytic function of POLD1 cannot be excluded and requires further investigation. Analysis of patients' T cells indicated the $POLD1^{R1060C}$ mutation impaired DNA replication and cell proliferation, an effect that was rescued by lentivirus-mediated expression of a WT but not the mutant $POLD1^{R1060C}$ protein. In contrast, B-cell proliferation was spared.

A key finding in our studies is that the $POLD1^{R1060C}$ mutation not only impaired T-cell proliferation but was also associated with restricted TCR V-J pairing and severe oligoclonality in $CD8^+$ T cells. Importantly, these abnormalities appeared limited to the $CD8^+$ T-cell compartment and did not involve the $CD4^+$ T or B cells. These findings suggest that Polδ differentially affects CD8 T cells, severely limiting their peripheral expansion and possibly affecting their thymic development. A differential effect of $POLD1^{R1060C}$ on the $CD8^+$ T-cell compartment would be consistent with the heightened susceptibility of the patients to herpetic and viral respiratory tract infections. In contrast, the patients have thus far been spared infections associated with severe $CD4^+$ T-cell depletion, such as *Pneumocystis jirovecii*. This sparing might reflect the continued presence of diverse but profoundly lymphopenic CD4 T-cell populations and the absence of concurrent debilitating diseases.

In contrast to the T-cell defects noted in the patients, the B-cell compartment appeared to be completely spared in terms of B-cell proliferation, *IgH* V-J pairing, D gene use, and SHM. Furthermore, indices, such as the proportion of tyrosine residue of the IGH-CDR3 region and the *IgH* hydrophobicity profile, both associated with B-cell self-reactivity, were either similar (the former) or marginally affected (the latter). In view of these findings, the presence of mild hypogammaglobulinemia in patients with waning antibody responses to vaccines that can be rescued by booster immunization is best explained by suboptimal T-cell help.

Previous studies have identified different heterozygous mutations affecting the catalytic and exonuclease domains of POLD1.[17,35,36] The former gives rise to a distinct multisystem development characterized by subcutaneous lipodystrophy, deafness, and mandibular hypoplasia, whereas the latter results in familial colorectal cancers. Interestingly, neither of these 2 types of POLD1 mutations resulted in immunodeficiency. In contrast, the kindred reported herein had very minimal manifestations aside from the immunodeficiency, notably partial sensorineural hearing loss in P1. This sharp segregation of disease phenotypes as a function of the respective domains targeted by mutations suggests the $POLD1^{R1060C}$ mutation, which locates away from the enzymatic domains, might allow for residual Polδ activities to rescue the multisystem and mutator phenotypes associated with catalytic and proofreading activities in different tissues. However, the Polδ complex might play a nonredundant role in protein-protein interactions with other components of the double-stranded break repair relevant to VDJ recombination in $CD8^+$ T cells. The nature of such interactions involving the Polδ complex in double-stranded break repair and their role in T-cell development requires further investigation.

In addition to the *POLD1* mutation reported herein, a splice junction mutation in DNA polymerase ε subunit 2 *(POLE2)* has been described in a child with dysmorphic features and combined immunodeficiency and autoimmunity, with an absence of circulating B cells, T-cell lymphopenia, and neutropenia.[37] POLE2 is an accessory subunit in the Polε complex,[38] and although the protein expression of mutant POLE2 was unaffected

in the child, the mutation might adversely affect the Polε complex assembly, its interactions with other proteins relevant to DNA replication, or both. The *TRB* repertoire in the patient with POLE2 appeared largely normal, indicating that the restricted V-J pairing in the *TRB* of $CD8^+$ T cells in the patients with the $POLD1^{R1060C}$ mutation was specific to this gene defect. Overall, these results point to an emerging subgroup of primary immunodeficiency disorders caused by genetic lesions in different DNA polymerases. The full spectrum of these disorders and their unique and shared attributes require further investigation.

Key messages

- **A POLD1 mutation disrupted the assembly of the Polδ complex and resulted in T-cell immunodeficiency.**
- **The patients' $CD8^+$ T cells exhibited severe oligoclonality and restricted TCR β-chain V-J pairing.**

REFERENCES

1. Coleman WB, Tsongalis GJ. Multiple mechanisms account for genomic instability and molecular mutation in neoplastic transformation. Clin Chem 1995;41:644-57.
2. Chilkova O, Stenlund P, Isoz I, Stith CM, Grabowski P, Lundstrom EB, et al. The eukaryotic leading and lagging strand DNA polymerases are loaded onto primer-ends via separate mechanisms but have comparable processivity in the presence of PCNA. Nucleic Acids Res 2007;35:6588-97.
3. Greenough L, Menin JF, Desai NS, Kelman Z, Gardner AF. Characterization of family D DNA polymerase from *Thermococcus* sp. 9 degrees N. Extremophiles 2014;18:653-64.
4. Henneke G, Flament D, Hubscher U, Querellou J, Raffin JP. The hyperthermophilic euryarchaeota *Pyrococcus abyssi* likely requires the two DNA polymerases D and B for DNA replication. J Mol Biol 2005;350:53-64.
5. Podust VN, Chang LS, Ott R, Dianov GL, Fanning E. Reconstitution of human DNA polymerase delta using recombinant baculoviruses: the p12 subunit potentiates DNA polymerizing activity of the four-subunit enzyme. J Biol Chem 2002;277:3894-901.
6. Makarova KS, Krupovic M, Koonin EV. Evolution of replicative DNA polymerases in archaea and their contributions to the eukaryotic replication machinery. Front Microbiol 2014;5:354.
7. Song J, Hong P, Liu C, Zhang Y, Wang J, Wang P. Human POLD1 modulates cell cycle progression and DNA damage repair. BMC Biochem 2015;16:14.
8. Uchimura A, Hidaka Y, Hirabayashi T, Hirabayashi M, Yagi T. DNA polymerase delta is required for early mammalian embryogenesis. PLoS One 2009;4:e4184.
9. Lee MY, Zhang S, Lin SH, Wang X, Darzynkiewicz Z, Zhang Z, et al. The tail that wags the dog: p12, the smallest subunit of DNA polymerase delta, is degraded by ubiquitin ligases in response to DNA damage and during cell cycle progression. Cell Cycle 2014;13:23-31.
10. Tumini E, Barroso S, Calero CP, Aguilera A. Roles of human POLD1 and POLD3 in genome stability. Sci Rep 2016;6:38873.
11. Murga M, Lecona E, Kamileri I, Diaz M, Lugli N, Sotiriou SK, et al. POLD3 is haploinsufficient for DNA replication in mice. Mol Cell 2016;63:877-83.
12. Zhou Y, Meng X, Zhang S, Lee EY, Lee MY. Characterization of human DNA polymerase delta and its subassemblies reconstituted by expression in the MultiBac system. PLoS One 2012;7:e39156.
13. Strzalka W, Ziemienowicz A. Proliferating cell nuclear antigen (PCNA): a key factor in DNA replication and cell cycle regulation. Ann Bot 2011;107:1127-40.
14. Daee DL, Mertz TM, Shcherbakova PV. A cancer-associated DNA polymerase delta variant modeled in yeast causes a catastrophic increase in genomic instability. Proc Natl Acad Sci U S A 2010;107:157-62.
15. Church DN, Briggs SE, Palles C, Domingo E, Kearsey SJ, Grimes JM, et al. DNA polymerase epsilon and delta exonuclease domain mutations in endometrial cancer. Hum Mol Genet 2013;22:2820-8.
16. Liu D, Frederiksen JH, Liberti SE, Lutzen A, Keijzers G, Pena-Diaz J, et al. Human DNA polymerase delta double-mutant D316A;E318A interferes with DNA mismatch repair in vitro. Nucleic Acids Res 2017;45:9427-40.
17. Palles C, Cazier JB, Howarth KM, Domingo E, Jones AM, Broderick P, et al. Germline mutations affecting the proofreading domains of POLE and POLD1 predispose to colorectal adenomas and carcinomas. Nat Genet 2013;45:136-44.
18. Weedon MN, Ellard S, Prindle MJ, Caswell R, Lango Allen H, Oram R, et al. An in-frame deletion at the polymerase active site of POLD1 causes a multisystem disorder with lipodystrophy. Nat Genet 2013;45:947-50.
19. Sasaki H, Yanagi K, Ugi S, Kobayashi K, Ohkubo K, Tajiri Y, et al. Definitive diagnosis of mandibular hypoplasia, deafness, progeroid features and lipodystrophy (MDPL) syndrome caused by a recurrent de novo mutation in the POLD1 gene. Endocr J 2018;65:227-38.
20. Schmitz-Abe K, Li Q, Rosen SM, Nori N, Madden JA, Genetti CA, et al. Unique bioinformatic approach and comprehensive reanalysis improve diagnostic yield of clinical exomes. Eur J Hum Genet 2019;27:1398-405.
21. Case DA, Babin V, Berryman JT, Betz RM, Cai Q, Cerutti DS, et al. AMBER 14. San Francisco: San Francisco: University of California; 2014.
22. Berendsen HJC, Grigera JR, Straatsma TP. The missing term in effective pair potentials. J Phys Chem 1987;91:6269-71.
23. Joung IS, Cheatham TE. Determination of alkali and halide monovalent ion parameters for use in explicitly solvated biomolecular simulations. J Phys Chem B 2008;112:9020-41.
24. Berendsen HJC, Postma JPM, Vangunsteren WF, Dinola A, Haak JR. Molecular-dynamics with coupling to an external bath. J Chem Phys 1984;81:3684-90.
25. Ryckaert J-P, Ciccotti G, Berendsen HJC. Numerical integration of the cartesian equations of motion of a system with constraints: molecular dynamics of n-alkanes. J Comput Phys 1977;23:327-41.
26. Alamyar E, Duroux P, Lefranc MP, Giudicelli V. IMGT((R)) tools for the nucleotide analysis of immunoglobulin (IG) and T cell receptor (TR) V-(D)-J repertoires, polymorphisms, and IG mutations: IMGT/V-QUEST and IMGT/HighV-QUEST for NGS. Methods Mol Biol 2012;882:569-604.
27. Carlson CS, Emerson RO, Sherwood AM, Desmarais C, Chung MW, Parsons JM, et al. Using synthetic templates to design an unbiased multiplex PCR assay. Nat Commun 2013;4:2680.
28. Robins HS, Campregher PV, Srivastava SK, Wacher A, Turtle CJ, Kahsai O, et al. Comprehensive assessment of T-cell receptor beta-chain diversity in alphabeta T cells. Blood 2009;114:4099-107.
29. Gupta NT, Vander Heiden JA, Uduman M, Gadala-Maria D, Yaari G, Kleinstein SH. Change-O: a toolkit for analyzing large-scale B cell immunoglobulin repertoire sequencing data. Bioinformatics 2015;31:3356-8.
30. Garcia-Diaz M, Bebenek K. Multiple functions of DNA polymerases. CRC Crit Rev Plant Sci 2007;26:105-22.
31. Doublie S, Zahn KE. Structural insights into eukaryotic DNA replication. Front Microbiol 2014;5:444.
32. Li CJ. Flow cytometry analysis of cell cycle and specific cell synchronization with butyrate. Methods Mol Biol 2017;1524:149-59.
33. Dolbeare F, Gratzner H, Pallavicini MG, Gray JW. Flow cytometric measurement of total DNA content and incorporated bromodeoxyuridine. Proc Natl Acad Sci U S A 1983;80:5573-7.
34. Podust VN, Tiwari N, Stephan S, Fanning E. RFC disengages from proliferating cell nuclear antigen (PCNA) upon sliding clamp formation, and PCNA itself tethers DNA polymerase delta to DNA. J Biol Chem 1998;273:31992-9.
35. Bertocci B, De Smet A, Berek C, Weill JC, Reynaud CA. Immunoglobulin kappa light chain gene rearrangement is impaired in mice deficient for DNA polymerase mu. Immunity 2003;19:203-11.
36. Bertocci B, De Smet A, Weill JC, Reynaud CA. Nonoverlapping functions of DNA polymerases mu, lambda, and terminal deoxynucleotidyltransferase during immunoglobulin V(D)J recombination in vivo. Immunity 2006;25:31-41.
37. Lieber MR. The polymerases for V(D)J recombination. Immunity 2006;25:7-9.
38. Elsayed FA, Tops CMJ, Nielsen M, Ruano D, Vasen HFA, Morreau H, et al. Low frequency of POLD1 and POLE exonuclease domain variants in patients with multiple colorectal polyps. Mol Genet Genomic Med 2019;7:e00603.

METHODS

WES and data analysis

WES data were processed through the VExP by using the BWA aligner (version 0.7.17) for mapping reads to the human genome (hg19) and Picard Tools (version 2.20.2) to mark/delete duplicate reads. Single nucleotide variants and small insertions/deletions were jointly called across all samples by using both GATK (multisample variant calling, version 4.1) and SAMTools (version 1.9). Furthermore, VExP was performed to annotate 21 relevant genetic databases (from allele frequency and gene-phenotype consortiums) and 23 coding/noncoding variant pathogenicity predictors into the output of the system.

Variant analysis was performed by using different inheritance models (assuming full penetrance) based on 3 filtering criteria. First, variants predicted to have a potential functional coding consequence, including stop-gain or stop-loss, splice-site disruption, insertion and deletion, and nonsynonymous were included.

Second, variants were filtered based on allele frequency in control populations (the gnomAD, ExAC, EVS, and 1000 Genomes Project databases and internal data from 2114 unaffected subjects from Boston Children's Hospital). Finally, the variants were further prioritized to include those with read depths of 10 times or greater and deleterious prediction (≥2 of 23 types of software, including PolyPhen, SIFT, FATHMM, and CADD). For pedigree-consistency analysis, VExP had verified consistency within all family members.

Homozygosity mapping

We used VExP to determine homozygous regions using WES data. In summary, the method uses a sliding window approach, 100 single nucleotide polymorphisms, and retained segments with a minimum of 98% homozygosity. Homozygous single nucleotide polymorphisms cannot be more than 100 Kb away from each other. Next, VExP joins all the homozygous regions by using several considerations, including regions with no genes or noncoding genes. It retains only segments in which observed homozygosity exceeds 3 cM and avoids the effect of residual population homozygosity that is likely innocuous and tolerated by natural selection. We use genetic, as opposed to physical, distance for all calculations. To calculate overall homozygosity for every sample, we sum all segments exceeding 3 cM. Homozygosity mapping is applied to the results from the whole family, obtaining overlapping homozygous regions between affected subjects, with no overlapping with unaffected samples (Fig E1 and Table E3).

REFERENCE

E1. Kyte J, Doolittle RF. A simple method for displaying the hydropathic character of a protein. J Mol Biol 1982;157:105-32.

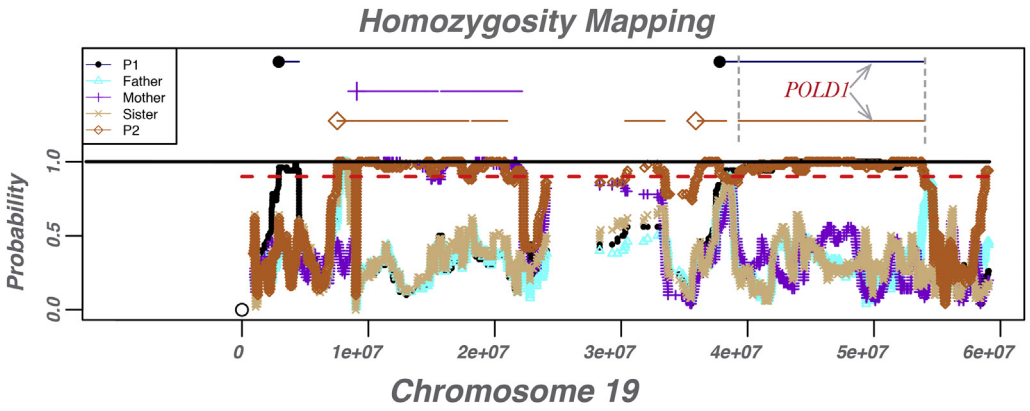

FIG E1. Homozygous regions identified in chromosome 19 by using WES and segregating within the family (homozygosity mapping).

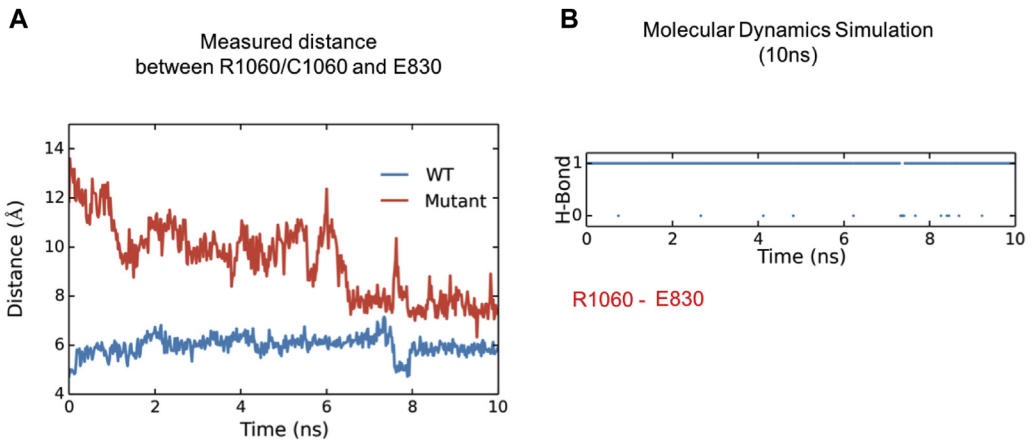

FIG E2. A, Distance measurement between residue 1060 and 830 in WT and mutant POLD1. Longer distance in the mutant POLD1 reflects interaction lost between the CysB and POLBc_delta domains. **B,** Hydrogen bond *(H-Bond)* tracing of the interaction between R1060 and E830 in POLD1: *1*, hydrogen bond exists; *0*, hydrogen bond disappears.

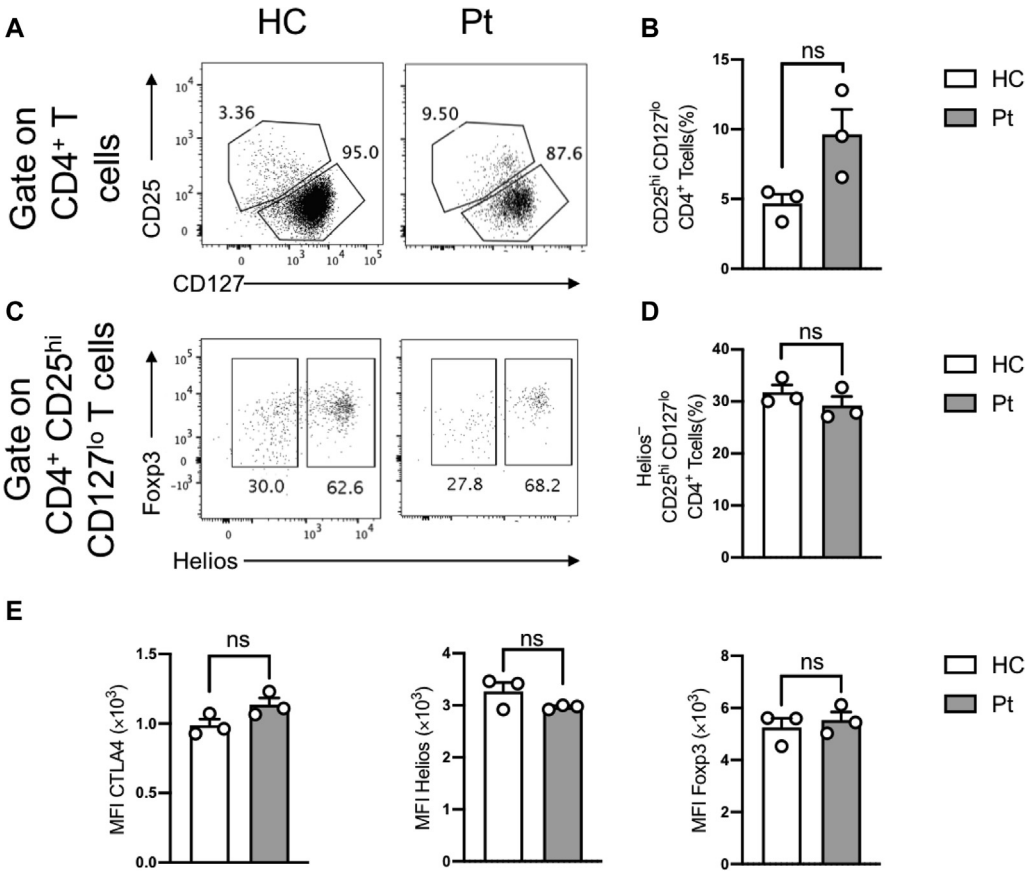

FIG E3. Patients with the POLD1^{R1060C} mutation have normal Treg cell frequencies and phenotypes. **A,** Representative dot plot analysis of CD25^{hi}CD127^{lo}CD4^{+} T cells in a patient *(Pt)* versus a healthy control subject *(HC)*. **B,** Percentages of CD25^{hi}CD127^{lo}CD4^{+} T cells in peripheral blood of healthy control subjects (n = 3; *open circles*) and patients with the POLD1^{R1060C} mutation (n = 3; *solid circles*). **C,** Representative dot plot analysis of Helios^{-}CD25^{hi}CD127^{lo}CD4^{+} T cells in a patient versus a control subject. **D,** Percentages of Helios^{-}CD25^{hi}CD127^{lo}CD4^{+} T cells in peripheral blood of healthy control subjects (n = 3; *open circles*) and patients with the POLD1^{R1060C} mutation (n = 3; *open circles*). **E,** Mean fluorescence intensity of the respective Treg cell marker in patients and control subjects. *ns,* Not significant (unpaired 2-tailed Student *t* test).

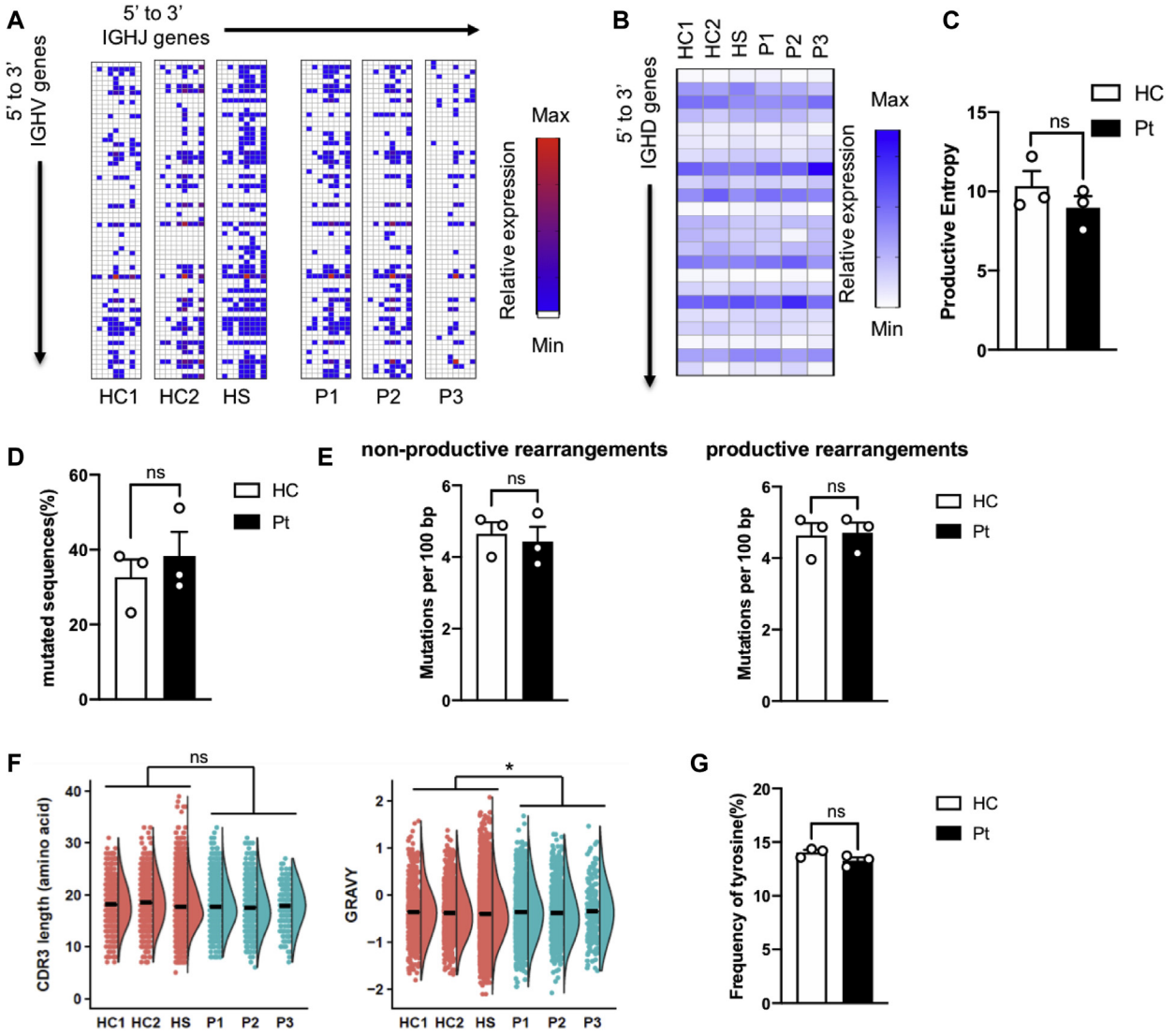

FIG E4. Profiles of IGHV-IGHJ pairing and SHM analysis in B cells from patients with the POLD1^{R1060C} mutation. **A,** Frequencies of specific IGHV and IGHJ pairing in unique *IGH* clonotypes of B cells from healthy control subjects *(HC)* and patients *(Pt)*. *White areas* represent the absence of a given IGHV and IGHJ pairing. *Blue areas* reflect a low frequency of usage, and *red areas* represent a higher frequency of usage. **B,** Frequencies of specific IGD gene usage in unique *IGH* clonotypes of B cells from healthy control subjects and patients. *White areas* represents the lowest gene usage. *Blue areas* reflects a higher frequency of usage. **C,** Productive entropy of B cells in healthy control subjects versus patients (n = 3; *open circles*). **D,** Percentage of sequences carrying at least 1 SHM among all unique rearrangements (productive and nonproductive) with resolved V families, genes, or alleles. **E,** Number of mutations per 100 bp within the IGH V segment of unique rearrangements, with at least 1 mutation in nonproductive rearrangements and productive rearrangements. **F,** Amino acid properties of the *in silico*–translated *IGH*-CDR3 region for unique productive rearrangements encoding a complete CDR3 region (starting and ending with consensus codons). CDR3 length: Control versus patient group, $P > .1$; subject effect, $P < 10e\text{-}6$. *GRAVY*, Grand average of hydrophobicity[E1]: Control versus patient group, $P = .0490$; subject effect, $P > .4$. **G,** Proportion of tyrosine residue in the *IGH*-CDR3 of unique sequences: Control versus patient group (n = 3; *open circles*). Fig E4, *C*, *D*, *E*, and *G*, were analyzed with the Student unpaired 2-tailed *t* test. Results represent means ± SEMs. *ns*, Not significant. Fig E4, *F*, was analyzed with 2-way ANOVA to contrast sequence patterns between patients and control subjects while accounting for per-subject variations. *ns*, Not significant. *$P < .5$.

TABLE E1. List of candidate variants identified by using WES (minor allele frequency ≤ 0.01) that segregate within the family (variants in P1 and P2 and not their unaffected sibling or parents)

Genetic model	Gene name	Exonic function	Amino acid change	Homozygosity	PolyPhen	SIFT
Recessive	*NADK*	Insertion (6 bases)	p.G414delinsRRG:p.G446delinsRRG: p.G591delinsRRG		NA	NA
Recessive	*FAT4*	Nonsynonymous	p.Q1257E		B	T
Recessive	*LY6G5C*	Nonsynonymous	p.F53L:p.F56L:p.F54L		B	T
Recessive	*AGER*	Nonsynonymous	p.G82S:p.G68S:p.G113S		P	T
Recessive	*NOTCH4*	Nonsynonymous	p.G294R		D	T
Recessive	*C6ORF10*	Nonsynonymous	p.G477V:p.G479V:p.G463V:p.G478V		D	D
Recessive	*C6ORF10*	Nonsynonymous	p.L264W:p.L266W:p.L250W:p.L257W:p.L265W		D	D
Recessive	*C6ORF10*	Nonsynonymous	p.G143R:p.G122R:p.G145R:p.G129R		NA	D
Recessive	*HLA-DRB5*	Stop-gain	p.Q220X		NA	NA
Recessive	*HLA-DRB1*	Nonsynonymous	p.V73M		D	D
Recessive	*HLA-DRB1*	Nonsynonymous	p.V73L		D	T
Recessive	*HLA-DRB1*	Nonsynonymous	p.D70N		D	D
Recessive	*HLA-DRB1*	Nonsynonymous	p.D57Y		P	D
Recessive	*HLA-DRB1*	Nonsynonymous	p.D57N		B	D
Recessive	*HLA-DQA1*	Nonsynonymous	p.M18T		B	T
Recessive	*TRAF3IP2*	Nonsynonymous	p.D10N:p.D19N		D	D
Recessive	*TULP4*	Nonsynonymous	p.S522N		B	T
Recessive	*GLT6D1*	Nonsynonymous	p.P219S		D	T
Recessive	*PITRM1*	Nonsynonymous	p.L64F:p.L441F:p.L785F:p.L883F:p.L884F		D	D
Recessive	*PITRM1*	Nonsynonymous	p.L113V:p.L145V		B	T
Recessive	*C14ORF178*	Nonsynonymous	p.G31D:p.G61D		B	D
Recessive	*C19ORF33*	Insertion (15 bases)	p.K90delinsKEGEGQ		NA	NA
Recessive	*GGN*	Nonsynonymous	p.A517V:p.A434V		D	T
Recessive	*RASGRP4*	Nonsynonymous	p.G165R		B	D
Recessive	*MIA*	Nonsynonymous	p.P16L	14.7 MB	NA	NA
Recessive	*PSG6*	Nonsynonymous	p.S312F:p.S405F	14.7 MB	B	D
Recessive	*PSG6*	Nonsynonymous	p.I122M:p.I243M	14.7 MB	D	D
Recessive	*ZNF221*	Nonsynonymous	p.V165M	14.7 MB	D	D
Recessive	*ZNF225*	Nonsynonymous	p.R352H	14.7 MB	D	D
Recessive	*CEACAM16*	Nonsynonymous	p.S32I	14.7 MB	B	D
Recessive	*RSPH6A*	Nonsynonymous	p.Q184H:p.Q448H	14.7 MB	D	D
Recessive	*POLD1*	Nonsynonymous	p.R1060C*	14.7 MB	D	D
Recessive	*SIGLEC12*	Nonsynonymous	p.A77T	14.7 MB	P	D
Compound heterozygous	*LRP1B*	Nonsynonymous	p.E3955K		B	T
Compound heterozygous	*LRP1B*	Nonsynonymous	p.V2146F		B	D
Compound heterozygous	*ZFHX3*	Nonsynonymous	p.Y865C		D	D
Compound heterozygous	*ZFHX3*	Nonsynonymous	p.K520N		B	T
De novo	*MUC12*	Nonsynonymous	p.S1610I:p.S1753I		B	D

PolyPhen and SFIT scores: *B*, benign; *D*, deleterious *P*, probably deleterious; *T*, tolerant.
NA, Not available.
*POLD1 R1060C is in reference to *POLD1* isoform 1 (NM_001256849.1).

TABLE E2. Summary of immune repertoire analysis

Sample	Cell input	Total templates	Unique clonotypes	Productive templates	Unique productive clonotypes
HC1-CD8	160,000	7,367	4,942	5,825	3,964
HC2-CD8	100,000	2,269	2,075	1,838	1,687
S002a-CD8	67,000	1,660	1,547	1,415	1,318
P002-CD8	93,000	2,568	243	1,653	187
S002b-CD8	50,000	1,401	496	910	416
P3-CD8	30,000	735	278	588	212
HC1-CD4	100,000	6,550	5,862	5,223	4,628
HC2-CD4	100,000	1,341	1,234	1,101	1,008
S002a-CD4	100,000	1,475	1,375	1,247	1,161
P002-CD4	64,000	4,528	3,655	3,693	2,936
S002b-CD4	100,000	2,046	1,964	1,773	1,703
P3-CD4	57,000	4,905	3,358	4,085	2,772
HC1-B	50,000	1,550	1,545	1,272	719
HC2-B	100,000	2,017	2,012	1,676	1,032
S002a-B	199,000	11,838	11,824	9,938	6,557
P002-B	28,000	3,148	3,143	2,604	1,359
S002b-B	75,000	1,652	1,643	1,294	770
P3-B	54,000	503	497	438	249

HC1, Healthy control subject 1; *HC2*, healthy control subject 2; *S002a*, healthy sibling; *P002*, patient 1; *S002b*, patient 2; *P3*, patient 3.

TABLE E3. Homozygous regions identified in autosomal chromosomes using WES and segregating within the family

Chromosome	Start position	End position	Size (MB)	Single nucleotide polymorphisms (homozygous)
3	130,098,639	132,105,588	2.007	262
6	33,032,788	38,650,628	5.618	1732
13	41,567,248	45,563,464	3.996	555
19	38,040,492	38,314,767	0.274	119
19	39,219,780	53,990,002	14.770	8617